ACS APPLIED ENERGY MATERIALS

www.acsaem.org Article

Carbon-Yarn-Based Supercapacitors with In Situ Regenerated Cellulose Hydrogel for Sustainable Wearable Electronics

José Tiago Carvalho, Inês Cunha, João Coelho, Elvira Fortunato, Rodrigo Martins, and Luís Pereira*

Cite This: *ACS Appl. Energy Mater.* 2022, 5, 11987−11996 Read Online

ACCESS | Metrics & More | Article Recommendations | Supporting Information

ABSTRACT: Developing sustainable options for energy storage in textiles is needed to power future wearable "Internet of Things" (IoT) electronics. This process must consider disruptive alternatives that address questions of sustainability, reuse, repair, or even a second life application. Herein, we pair stretch-broken carbon fiber yarns (SBCFYs), as current collectors, and an *in situ* regenerated cellulose-based ionic hydrogel (RCIH), as an electrolyte, to fabricate 1D fiber-shaped supercapacitors (FSCs). The areal specific capacitance reaches 433.02 $\mu F \cdot cm^{-2}$ at 5 $\mu A \cdot cm^{-2}$, while the specific energy density is 1.73 × 10^{-2} $\mu Wh \cdot cm^{-2}$. The maximum achieved specific power density is 5.33 × 10^{-1} $mW \cdot cm^{-2}$ at 1 $mA \cdot cm^{-2}$. The 1D FSCs possess a long-life cycle and 92% capacitance retention after 10 000 consecutive voltammetry cycles, higher than similar ones using the reference PVA/H_3PO_4 gel electrolyte. Additionally, the feasibility and reproducibility of the produced devices were demonstrated by connecting three devices in series and parallel, showing a small variation of the current density in flat and bent positions. An environmentally responsible approach was implemented by recovering the active materials from the 1D FSCs and reusing or recycling them without compromising the electrochemical performance, thus ensuring a circular economy path.

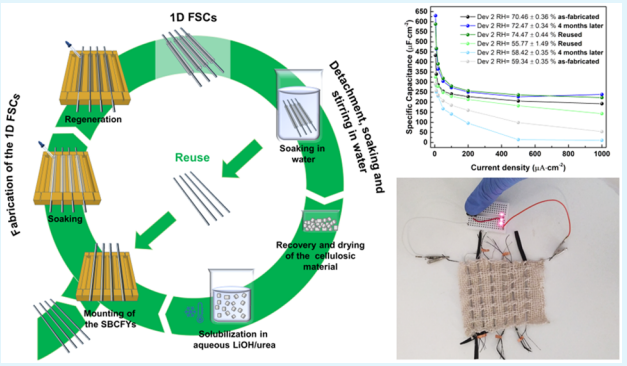

KEYWORDS: *cellulose, carbon fibers, fiber-shaped, energy storage, supercapacitor, sustainability*

1. INTRODUCTION

Robust, safe, and portable textile electronic devices that can interface with the human body and withstand extreme mechanical deformations while maintaining their performance are now at the heart of emerging concepts, such as smart wearables and the "Internet of Things" (IoT).[1,2] However, the uncontrollable consumption of this new generation of IoT gadgets, fed mostly by mass media and advertisements that encourage consumers to replace existing products with new ones, turns them obsolete quickly despite still being fully functional. A similar pattern is observed when considering the textile and clothing industry. Therefore, an additional requirement when producing, integrating, and disposing electronic devices that are integrated in/on textiles is to design a sustainable strategy by following a circular economy path that prioritizes reuse, repairing, and recycling.[3−5] Moreover, fibers/textiles that can store and release electrical energy are indispensable to effectively power integrated electronic systems for wearable smart clothing, capable of detecting and monitoring human activity/health and environmental conditions. Several energy-storage devices, namely, supercapacitors (SCs), have already been demonstrated in/on fiber/textile substrates (e.g., cotton fibers,[6,7] carbon fibers/yarns,[8−12] polymer fibers,[13] ultrafine metal fibers[14]).[15−17] The SCs stand out as promising energy-storage devices since they display higher power density, fast charging−discharging rate, long lifecycle, and good safety when compared to batteries.[18,19]

Flexible electrodes made of conductive fibers (e.g., metal wires, carbon fibers/yarns, conductive polymers, metal oxides, and hybrid/composite materials) are one of the key components needed to realize fiber-shaped SCs (FSCs) that can be further integrated into fabrics by traditional textile technologies (e.g., weaving, knitting, and embroidering).[20] Those fabricated with flexible carbon-based fibers/yarns and fabrics, which are biocompatible and environmentally friendly, are extremely appealing due to their high surface area, good electrical conductivity, high mechanical strength, chemical/thermal stability, and stability upon cycling. Moreover, they can be used as a binder and as current collector-free electrodes and are easily functionalized to fabricate 1D yarns, 2D fabrics, and 3D woven structures. They are available on the market and

Received: April 23, 2022
Accepted: August 12, 2022
Published: October 12, 2022

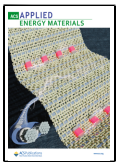

their manufacturing process, despite being well-established, is constantly being adapted to bring new functionalities.[21] In contrast, the nonelectrochemical active metal wire/fibers (e.g., Ti, Cu, Ni, and Au) are less flexible, do not contribute directly to the capacitance, and are heavy, which reduces the specific capacitance and energy density and also leads to poor wearability.[10,22]

The electrolyte, sandwiched between both fiber-shaped electrodes, also plays a crucial role in developing flexible and wearable technologies. Safe, conformable, and environmentally friendly ionic hydrogels based on polymeric frameworks soaked with electrolytic species have become one of the most desirable alternatives to flammable and toxic liquid organic electrolytes. In this sense, cellulose, the most abundant biopolymer in nature, has garnered much attention as a sustainable raw material to power future flexible energy-storage applications and as an alternative to petroleum-derived synthetic polymers.[23,24] The charged hydrophilic functional groups can be used to prepare cellulose-based hydrogels through their dissolution followed by physical and/or chemical cross-linking.[25,26] One suitable approach to obtain hydrogels consists of dissolving native cellulose in aqueous alkali hydroxide solvent systems combined with additives, such as PEG, urea, and/or thiourea, when precooled to temperatures below −5 °C.[27] This route fits the compromise of environmental awareness as it is fast, nonpolluting, easy to handle, and uses common chemicals that do not produce any hazardous byproducts.

In this work, we designed and prepared flexible 1D FSCs composed of flexible and recyclable ionic hydrogels that were produced through the dissolution of cellulose in a precooled aqueous lithium hydroxide (LiOH)/urea solvent system, followed by an *in situ* regeneration process directly on carbon fiber yarn electrodes. The methodology used to produce the 1D FSCs allows for the recovery of both electrodes and electrolytes, ensuring a fully sustainable energy-storage fiber system made of reused/recycled materials for wearable IoT electronics.

2. EXPERIMENTAL SECTION

2.1. Materials and Chemicals. Microcrystalline cellulose (MCC) (Sigma-Aldrich, powder: 20 μm); LiOH (Sigma-Aldrich, ≥98%); urea (Carl Roth, ≥99.5%); deionized water (Millipore); glacial acetic acid (Sigma-Aldrich, ≥99); PVA (Sigma-Aldrich, $M_w \approx 61\,000$); phosphoric acid (H_3PO_4, Fluka, ≥85%); and table salt sodium chloride (NaCl) were used. SIGRAFIL stretch-broken carbon fiber yarns (SBCFYs, reference C SB70-3.3/240-R100; fineness of yarn: 70 tex (2 × 35)) were obtained from the SGL Group − The Carbon Company; cotton yarn 20 tex from Spinnerei C. B. Goldner GmbH & Co. KG; acrylonitrile butadiene styrene (ABS) from Ultimaker; and polydimethylsiloxane (PDMS, SYLGARD 184 Silicone Elastomer) and the respective curing agent from Dow Corning in a fixed 10 to 1 mix ratio.

2.2. Preparation of the PVA/H_3PO_4 Electrolyte Solution. The PVA/H_3PO_4 electrolyte solution was prepared by mixing 3 g of PVA in 30 mL of deionized water and heated to 80 °C under stirring until the solution became clear. Subsequently, 1.5 mL of H_3PO_4 was carefully added to the previous solution and allowed to reach room temperature under stirring, before being used.

2.3. Solubilization of Cellulose in the Aqueous LiOH/Urea Solvent System. Inspired by the procedures reported in the literature,[28−32] the cellulose dissolution medium was prepared by mixing 4.6 wt % of LiOH (0.46 g, Sigma-Aldrich, ≥98%) and 15 wt % of urea (1.5 g, Carl Roth, ≥99.5%) in 80.4 wt % deionized water (8.04 g, Millipore). The solvent mixture was precooled in a freezer at −25 °C until it became a frozen solid. The frozen solution was then allowed to thaw at ambient conditions, and 5 wt % of MCC (0.5 g, Sigma-Aldrich, powder: 20 μm) was slowly added into the solvent system (9.5 g) under vigorous stirring at −8 °C until its complete dissolution (≈30 min). A freezing−thawing cycle was performed to improve cellulose dissolution. The transparent solution was kept overnight in a freezer at −25 °C until further use.

2.4. Fabrication of Fiber-Shaped Supercapacitors. Flexible 1D FSCs were fabricated with a planar configuration, using commercially available SBCFY electrodes with a length size of 7 cm. Cotton yarn was twisted over one of the SBCFY electrodes with a winding/spiraling machine TS4 from Bocca Comorio Srl, serving as the separator.

The two SBCFYs were aligned in parallel in a 3D-printed ABS mold coated with a chemical resistant layer of PDMS, where they were fixed to be firmly stretched and held together during the coating and drying steps.

The cellulose-based ionic hydrogel was obtained from a solution composed of solubilized MCC that was removed from the freezer and left to thaw at RT. Then, 1 mL of the solution was poured into each cavity of the mold, where the SBCFYs were kept immersed with the electrolytic solution for 1 h at −8 °C. An *in situ* regeneration was performed at ambient conditions by placing 2 mL of pure glacial acetic acid directly into the solubilized MCC solution, which turns into a hydrogel surrounding the SBCFYs. The immersion in acetic acid was performed at different times (5, 10, 20, 30, and 60 min). The as-prepared devices were allowed to dry in the mold, overnight (22 °C, 45% RH).

For the fabrication of FSCs with PVA/H_3PO_4 gel electrolyte, each cavity of the ABS/PDMS mold was filled with 1 mL of the electrolyte solution, and the two electrodes were dip-coated together 5 times for 25 min. Between each dip-coating step, the solution was removed, and the SBCFYs coated with the electrolyte were partially dried with a hairdryer. The as-prepared devices were kept under ambient conditions.

Concerning the end-of-life, the fabricated FSCs were thoroughly washed with deionized water to remove the remaining salts from the regenerated cellulose-based ionic hydrogels (RCIHs). The soaked hydrogels were detached from the SBCFYs, and the recovered materials were dried at 40 °C for 6 h and stored at ambient conditions for 1 day before being used. The dried regenerated cellulosic material was reused to prepare a solution composed of 5 wt % of recovered material in a precooled aqueous LiOH/urea solvent system, using the solubilization strategy previously used for MCC. The recovered SBCFYs were reused to fabricate new planar FSCs using the recycled cellulose-based electrolytic solution. The fabrication procedure was identical with the one used for pristine devices.

2.5. Morphological, Chemical, Thermal, and Structural Characterization. An optical stereomicroscope (Leica M80) was used to visualize the appearance of the produced FSCs.

The morphology of the produced devices was examined by scanning electron microscopy (SEM) using a Carl Zeiss AURIGA CrossBeam FIB-SEM workstation and Hitachi TM3030Plus tabletop workstation.

Fourier transform infrared spectroscopy analysis (FTIR) was used to study the chemical composition of the resulting hydrogels. The spectra were acquired at room temperature between 4000 and 550 cm^{-1} with 4 cm^{-1} using a Thermo-Nicolet 6700 spectrophotometer from the Thermo Electron Corporation operating in attenuated total reflection (ATR) mode. These results were correlated with X-ray diffraction (XRD) measurements using a PANalytical X'Pert Pro, with Bragg−Brentano geometry and Cu Kα line radiation (λ = 1.5406 Å).

Contact angle (CA) measurements were carried out with equipment from DataPhysics (OCA15plus), using 1 μL drops of deionized water on five different places on the RCIH membrane (RH = 33%), and five measurements were acquired to determine an average value of CA (left and right).

2.6. Electrochemical Characterization. The electrochemical characterization of the planar 1D FSCs was made using a Gamry Instruments Reference 600 Potentiostat. Before starting the electro-

https://doi.org/10.1021/acsaem.2c01222
ACS Appl. Energy Mater. 2022, 5, 11987−11996

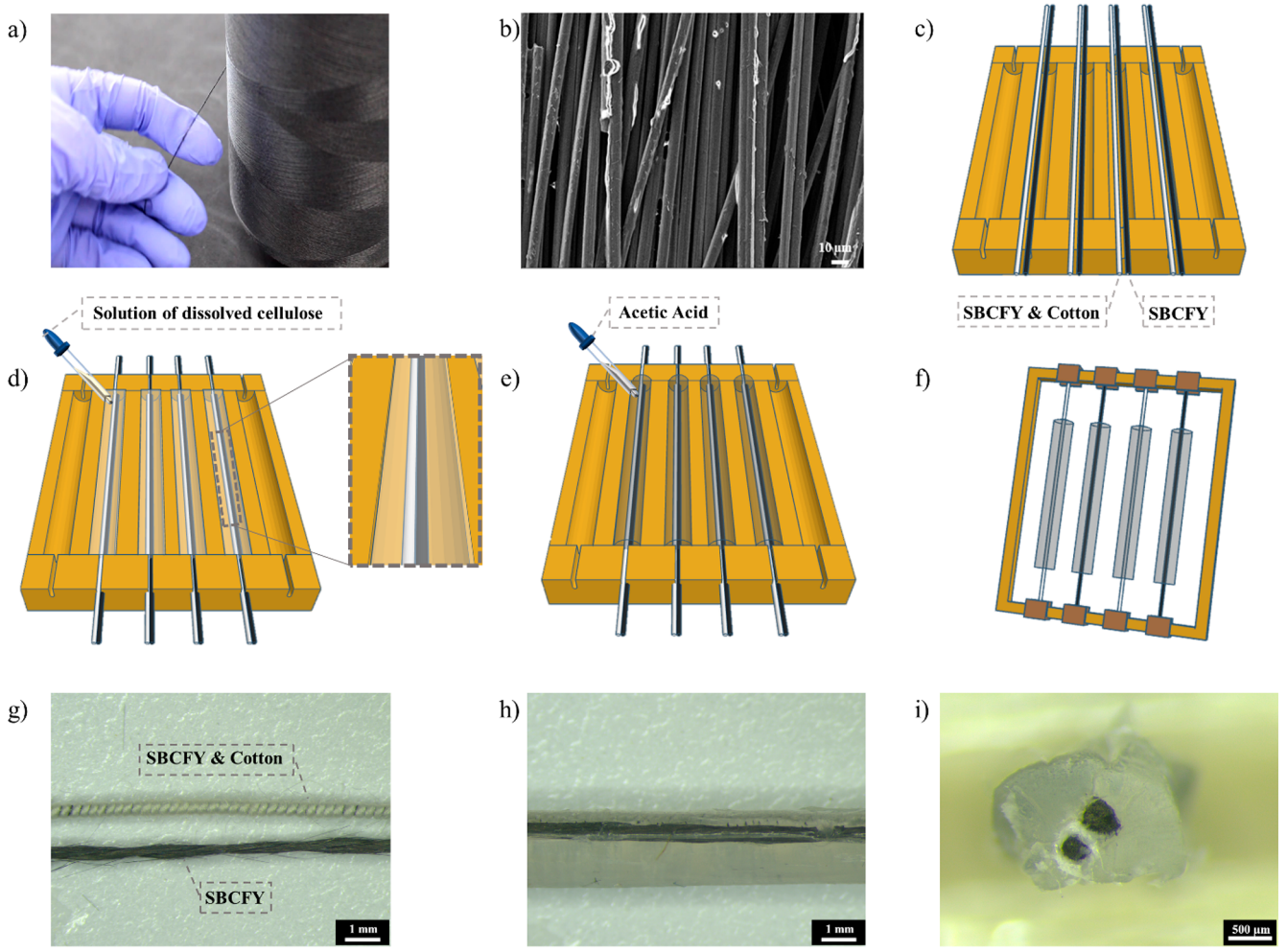

Figure 1. (a) Photograph of a commercial SIGRAFIL stretch-broken carbon fiber yarn (SBCFYs) roll and (b) respective high-magnification SEM image. Schematic representation of the manufacturing process of the 1D planar FSCs coated with an *in situ* RCIH. (c) The SBCFY and the SBCFY twisted with cotton in the cavity of the 3D-printed ABS/PDMS mold. (d) Soaking process of the SBCFYs with MCC solution. (e) *In situ* regeneration with glacial acetic acid and (f) the drying of the devices. (g) Optical images of single SBCFYs coated with cotton, (h) the fabricated FSC, and (i) the respective cross-section image.

chemical measurements, the devices were stored overnight under a controlled environment to stabilize their RH level. The devices were stored under two distinct RH conditions: 56−58% and 70−74% (achieved with saturated aqueous NaCl solution). The ambient conditions were continuously monitored by a Velleman CM2302/DHT22 humidity/temperature sensor connected to an Arduino during the device's characterization. A similar approach was conducted for the samples using PVA/H_3PO_4 electrolyte.

Cyclic voltammetry (CV) measurements were performed for different scan rates ranging from 5 to 10 000 mV·s^{-1}. Electrochemical impedance spectroscopy (EIS) measurements were performed at open-circuit potential (OCP) with a 5 mV AC voltage amplitude in a frequency range from 100 kHz to 10 mHz. Galvanostatic charge−discharge (GCD) measurements were carried out in chronopotentiometry mode at current densities of 5, 10, 20, 50, 100, 200, 500, and 1000 μA·cm^{-2}.

Retention tests were carried out by performing consecutive CV measurements for 10 000 cycles at 1000 mV·s^{-1}. For this study, the areal capacitance was determined as a function of the yarn's geometric area (0.68 cm^2), considering the outside of it, as represented in Figure S1.

3. RESULTS AND DISCUSSION

3.1. Characterization of Stretch-Broken Carbon Fiber Yarns. Commercial discontinuous stretch-broken carbon fiber yarns (SBCFYs) (Figure 1a,b) from SGL carbon, compatible with textile processes and obtained from polyacrylonitrile (PAN) fibers, were used as binder- and current collector-free electrodes to design 1D FSCs. Due to the good electrical conductivity, superior thermal and chemical stability, high tensile strength, remarkable flexibility (Figure S2), and low mass density, carbon fibers are very attractive for wearable applications.[21,33−35] As illustrated in Figure 1c, the 1D FSCs were fabricated with a planar structure by placing two SBCFYs side by side inside a mold container, where they were kept fixed, aligned, and firmly stretched during the entire manufacturing process. The active length of each SBCFY is 7 cm, while the gap between both SBCFYs was established by the cotton yarn separator that was twisted around one of the SBCFYs, which also avoids possible short circuits from "disheveled" fibers coming out from the SBCFYs. Then, they were soaked in solubilized microcrystalline cellulose (MCC) solution (Figure 1d), which was *in situ* regenerated directly on the SBCFYs by adding pure glacial acetic acid (Figure 1e), simplifying both the design and manufacturing process. The fabricated 1D FSCs (Figure 1f) were then carefully removed from the mold and transferred to a support. They were kept aligned in the vertical position and firmly stretched during the

https://doi.org/10.1021/acsaem.2c01222
ACS Appl. Energy Mater. 2022, 5, 11987−11996

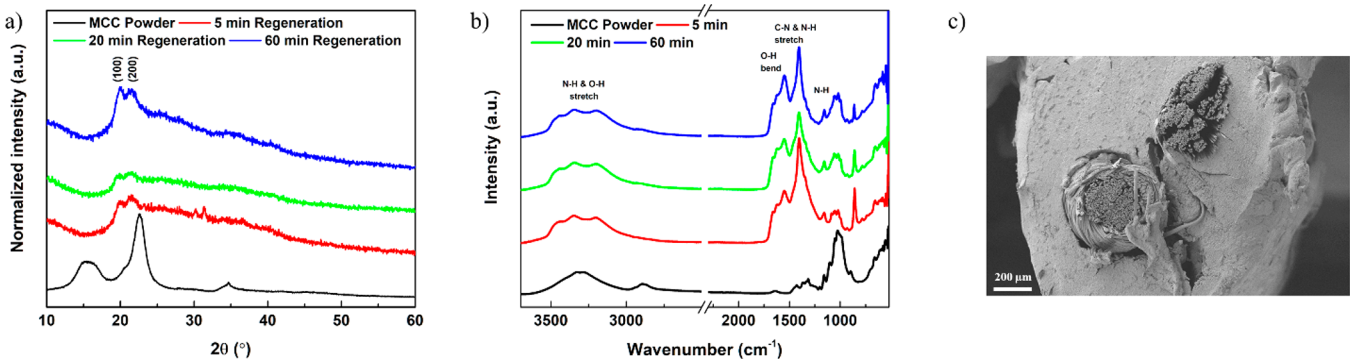

Figure 2. Characterization of the RCIHs obtained after different regeneration times: (a) XRD diffractograms after being regenerated in glacial acetic acid (MCC is given for comparison), (b) the respective FTIR spectrum, and (c) SEM cross-section image of the fabricated 1D planar FSCs, where is it possible to visualize both SBCFYs and the regenerated RCIH.

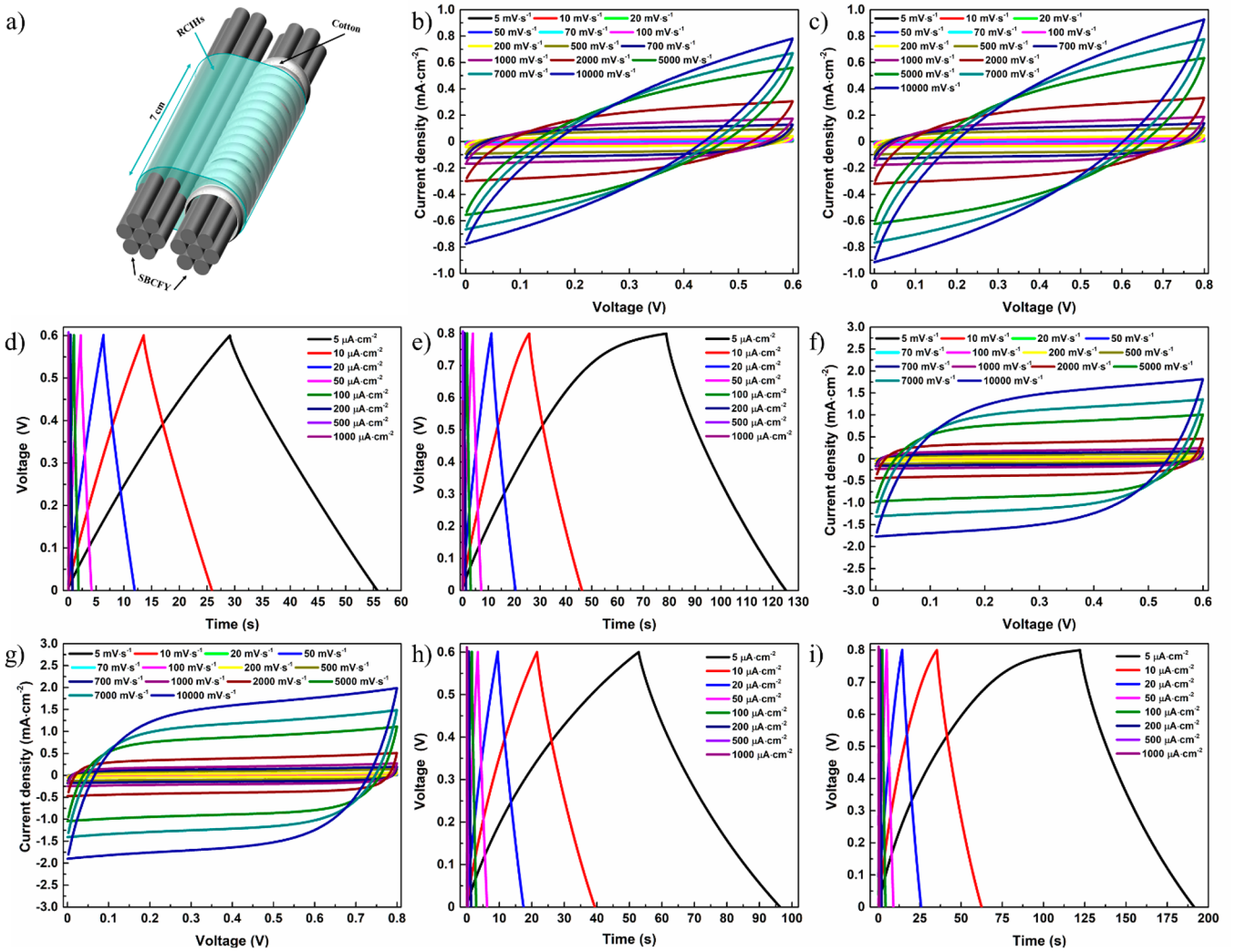

Figure 3. (a) Schematic representation of the 1D FSCs. CV curves of a single 1D FSC at different scan rates, ranging from 5 to 10 000 mV·s^{-1} for a voltage window of (b) 0.6 V and (c) 0.8 V. (d and e) Correspond to the GCD curves for the relative humidity (RH) level of 59.34 ± 0.35%, respectively. (f and g) CV and (h and i) GCD curves of the same 1D FSCs for an RH level of 70.46 ± 0.36%, respectively.

drying procedure carried out overnight under ambient conditions. Figure 1g,i shows the SBCFYs as well as the fabricated device and the respective cross-section image.

3.2. *In Situ* Regeneration of Cellulose-Based Ionic Hydrogels. The dissolution of highly crystalline MCC in aqueous alkali salt/urea solution at low temperature (<0 °C) was used to produce regenerated cellulose-based ionic hydrogel (RCIH) electrolytes. The mechanism behind the dissolution of cellulose under such conditions relies on creating a stable inclusion complex, consisting of hydrogen-bonded networks between cellulose, alkali hydroxide, urea, and water, which also aids in the reduction of the entanglement and self-

https://doi.org/10.1021/acsaem.2c01222
ACS Appl. Energy Mater. 2022, 5, 11987−11996

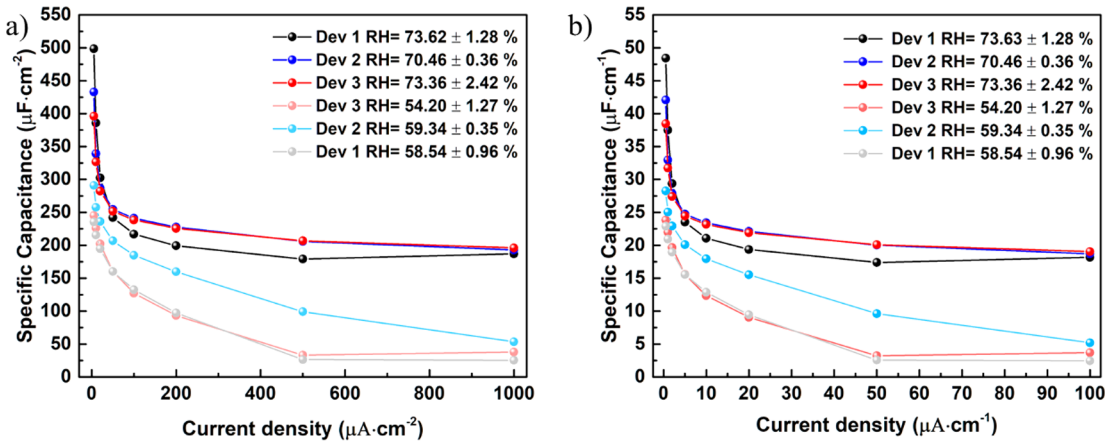

Figure 4. (a) Variation of the areal and (b) the length-specific capacitances measured at different current densities, ranging from 5 to 1000 $\mu A \cdot cm^{-2}$ and 0.5 to 100 $\mu A \cdot cm^{-1}$, for three 1D fiber-shaped supercapacitors at two RH levels, within an operating voltage window of 0.8 V, respectively.

association of the cellulose chains.[29,36−39] The alkali hydroxide salt chosen for cellulose dissolution was LiOH, due to its superior dissolution efficiency compared to NaOH.[38,39] As illustrated in Figure 1d, the solution was poured into the container, where the electrodes were kept immersed for 60 min at −8 °C to ensure a uniform coating with the electrolytic solution. This step is advantageous to promote the soaking of the cotton yarn while ensuring the establishment of a good interface between the hydrogel obtained after regeneration and the electrodes. The *in situ* regeneration process (Figure 1e) was triggered by soaking the solubilized MCC solution with glacial acetic acid, thus inducing the self-aggregation of cellulose to readily form physical regenerated cellulose hydrogel with the exact shape of the mold cavities.[29,40] It is important to mention that the regeneration process is not fully interrupted after removing the samples from the container since the hydrogel is heavily soaked with acetic acid. Therefore, the regeneration is only finished when the excess solvents have been completely evaporated from the hydrogels. As observed in previous works,[30,31] this approach is very appealing to provide ionic species, such as lithium alkali cations, in the regenerated cellulose matrix.

The XRD diffractograms obtained for the hydrogels prepared with different regeneration times (Figure 2a) reveal two peaks at 20 and 21.7° for (110) and (200) planes, respectively, assigned to cellulose II, which is common for regenerated cellulose.[39,41] Fast regeneration times lead to the formation of nonuniform hydrogels along the SBCFYs, establishing a poor interface between the electrodes and the electrolyte. On the other hand, longer regeneration times improved the interface integrity.

FTIR spectra of the prepared RCIHs are displayed in Figure 2b, and the spectrum of MCC powder is used as a reference. An overlapping of bands occurs in the range of 3600−3000 cm^{-1} related to the N−H stretching vibration of urea molecules (asymmetric stretching at 3449 cm^{-1} and symmetric stretching at 3342 cm^{-1}) and the O−H stretching vibration of water molecules.[42,43] A characteristic band of cellulose II is evidenced by the shoulder band at 3448 cm^{-1}, which is assigned to O−H groups forming intramolecular hydrogen bonds.[41] Additional overlapped bands are visible in the region between 1750 and 1520 cm^{-1}, corresponding to the O−H bending vibration of water molecules as well as amide I and amide II of urea molecules. The band at 1456 cm^{-1} is attributed to the C−N asymmetric stretching and N−H deformation of amide III, while the overlapping band at 1157 cm^{-1} is assigned to the rocking vibration of NH_2.[42,43] Therefore, the optimal regeneration time for the RCIHs was found to be 60 min as they ensure the full conversion of cellulose I into cellulose II and the formation of a reasonably uniform and conformable coating of the planar SBCFYs electrodes (Figure 1h,I and Figure 2c).

3.3. Electrochemical Performance of the 1D Fiber-Shaped Supercapacitors. The first step in determining the electrochemical performance and the underlying storage mechanism (electrical double layer (EDL) or pseudocapacitance) was to establish an electrochemically stable potential window (ESPW).[44,45] Figure S3 shows the evolution of the working voltage window of the 1D FSCs. A stable voltammogram is obtained after performing 10 consecutive CV cycles at 5 $mV \cdot s^{-1}$. The quasi-rectangular behavior, characteristic of the EDL, starts deforming around 0.6−0.8 V. The charged hydrophilic functional groups in combination with ionic species incorporated during the RCIH preparation are responsible for swelling and water retention.[26] It is well-known that aqueous electrolytes display a narrow operation voltage window below 1.23 V due to the water hydrolysis.[46]

After establishing the ESPW, the CV, GCD, and EIS characteristics were obtained in a two-electrode configuration (Figure 3a). Figure 3 shows the CV curves of a single device at different scan rates, from 5 to 10 000 $mV \cdot s^{-1}$, in a voltage window of 0−0.6 and 0−0.8 V for two distinct relative humidity (RH) levels.

The symmetrical quasi-rectangular shapes of the CVs, characteristic of the carbon electrode materials, reflect the ideal electrical double-layer capacitive (EDLC) behavior, which relies on adsorption/desorption of ionic chargers at the electrode/electrolyte interfaces.[44] At an RH level of 59.34%, the quasi-rectangular behavior is limited for a scan rate of 2000 $mV \cdot s^{-1}$ (Figure 3b−e), while for RH = 70.46% it is preserved at 10 000 $mV \cdot s^{-1}$ (Figure 3f−i). The hydrophilic nature of the RCIHs and their porous 3D structure improve the ionic conductivity at higher RH.[45] The measured left and right CAs of a RCIH membrane were 18.36 ± 1.64° and 17.36 ± 0.97°, respectively, indicating its high hydrophilicity. Regarding the ionic conductivity (Figure S4), the RCHI membrane exhibits a value of 5.61×10^{-4} and 1.23×10^{-3} $S \cdot cm^{-1}$ for RH = 60.13 and RH = 78.50%, respectively.

https://doi.org/10.1021/acsaem.2c01222
ACS Appl. Energy Mater. 2022, 5, 11987−11996

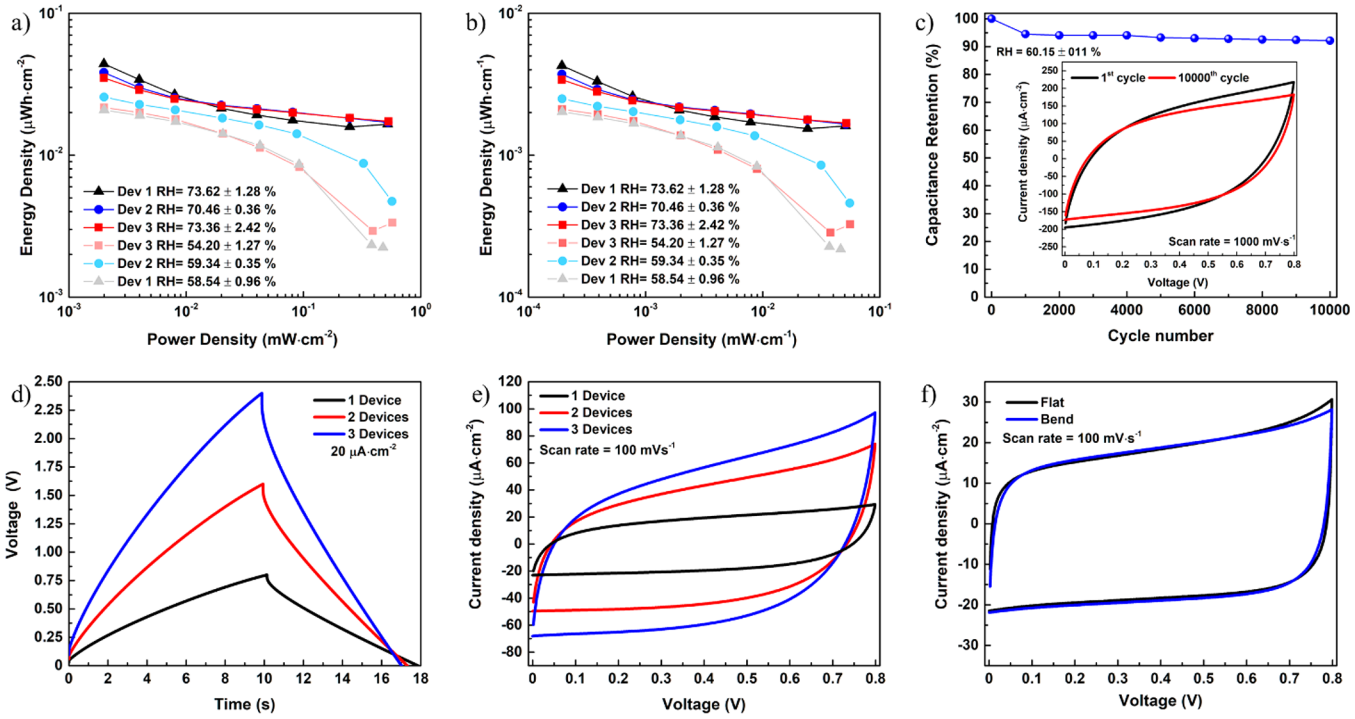

Figure 5. Ragone plots (a and b) of the three 1D FSCs subjected to both RH levels, (c) the cycling performance at a scan rate of 1000 mV·s^{-1} for 10 000 CV cycles, in a voltage window of 0.8 V and for a RH of 60.15 ± 0.11%, (d) GCD profiles of three 1D FSCs in series at 20 μA·cm^{-2}, (e) the CV curves of three devices in parallel at 100 mV·s^{-1}, and (f) the CV of the device in flat and bent positions.

The respective GCD curves exhibit triangular forms confirming the ideal capacitive behavior. For a voltage window of 0.8 V and a current density of 5 μA·cm^{-2} (Figure 3e and 3i), it is possible to verify a plateau that can be related to an overcharge of the device by exceeding the limit of the ESPW, thus leading to parasitic side reactions and unwanted decomposition of the electrolyte.[44]

Figure 4 depicts the specific capacitance (C_s), per area and length, over the applied current densities for three 1D FSCs, considering both RH levels and an operating voltage window of 0.8 V. Figure S5 shows the C_s for an operating voltage window of 0.6 V. As specified in Table S1, the device reaches a C_s of 498.48 μF·cm^{-2} at 5 μA·cm^{-2} for an RH level around 70%. Even at high current densities of 1 mA·cm^{-2}, the devices can retain a C_s of 180 μF·cm^{-2}. The adopted linear configuration provides a small interface area, while the twisted cotton yarn increases the distance between both SBCFY electrodes. At the same time, its presence is crucial to avoid possible short circuits from disheveled carbon fibers. Additionally, it may limit the active surface area of the 1D FSCs, hindering the impregnation of RCIHs and reducing the contact points with the SBCFY. Nevertheless, it is expected that for higher RH the hydrophilic character of the RCIH results in improved ionic conductivity and improved interfacial contact with the SBCFY, leading to an increase in the C_s.

Additionally, we have evaluated the electrochemical performance of 1D FSCs with PVA/H_3PO_4 gel electrolyte. Electrolytes based on PVA mixed with acidic or neutral mediums are commonly reported in the literature to test the reliability of SCs. They are known to provide a voltage window that can be extended up to 1 V and give some flexibility and stretchability to the devices.[45] For this specific case, the PVA/H_3PO_4 gel electrolyte was deposited around the SBCFYs, by executing five dip-coating steps. The devices were tested after partial drying and the day after in a controlled RH environment. Figure S6a,b depicts the CV of one characterized device where it is possible to confirm the degradation of its electrochemical performance, in just 1 day, after placing the device in a controlled RH environment. The as-fabricated device could reach a specific capacitance of 353.03 μF·cm^{-2} at 5 μA·cm^{-2} for a voltage window of 0.8 V, which is higher than the values determined for the devices based on RCIHs. The C_s decays to 190.91 μF·cm^{-2} in the controlled RH environment. The quasi-rectangular behavior is not preserved for high scan rates, while the devices cannot sustain such high current densities, as can be seen on the GCD curves. This could be related to the insufficient hydrophilic side chain groups in PVA, which will not support water retention and impair the long-term stability of the devices.[45]

The ESR was determined from the Nyquist plot using the real part of the complex impedance at 1 kHz.[47] The Nyquist, bode plot, and phase angle of one 1D FSC, tested from 100 kHz to 0.01 Hz at open-circuit voltage, are shown in Figure S7. The ESR values for three devices are summarized and compared in Table S1. The ESR of device 2 decreases from 200 to 58.89 Ω, increasing the RH level from 59.34 to 70.46%. This increase in the RH also influences the phase angle. In addition, the ESR values determined from the EIS are lower than those determined from GCD, as expected.[47] From Figure S7c, it is also possible to verify that the devices' capacitive domain is dependent on the frequency.

Figure 5a,b shows the Ragone plots to compare the energy and power density of the RCIH 1D FSCs for different RH levels and operation voltage windows. Considering the operating voltage window of 0.8 V, the maximum energy density was 3.35 × 10^{-3} μWh·cm^{-2} at 5.74 × 10^{-1} mW·cm^{-2} and 4.78 × 10^{-4} μWh·cm^{-1} at 8.19 × 10^{-2} mW·cm^{-1}. Maintaining the RH level of around 70%, the energy density is

https://doi.org/10.1021/acsaem.2c01222
ACS Appl. Energy Mater. 2022, 5, 11987−11996

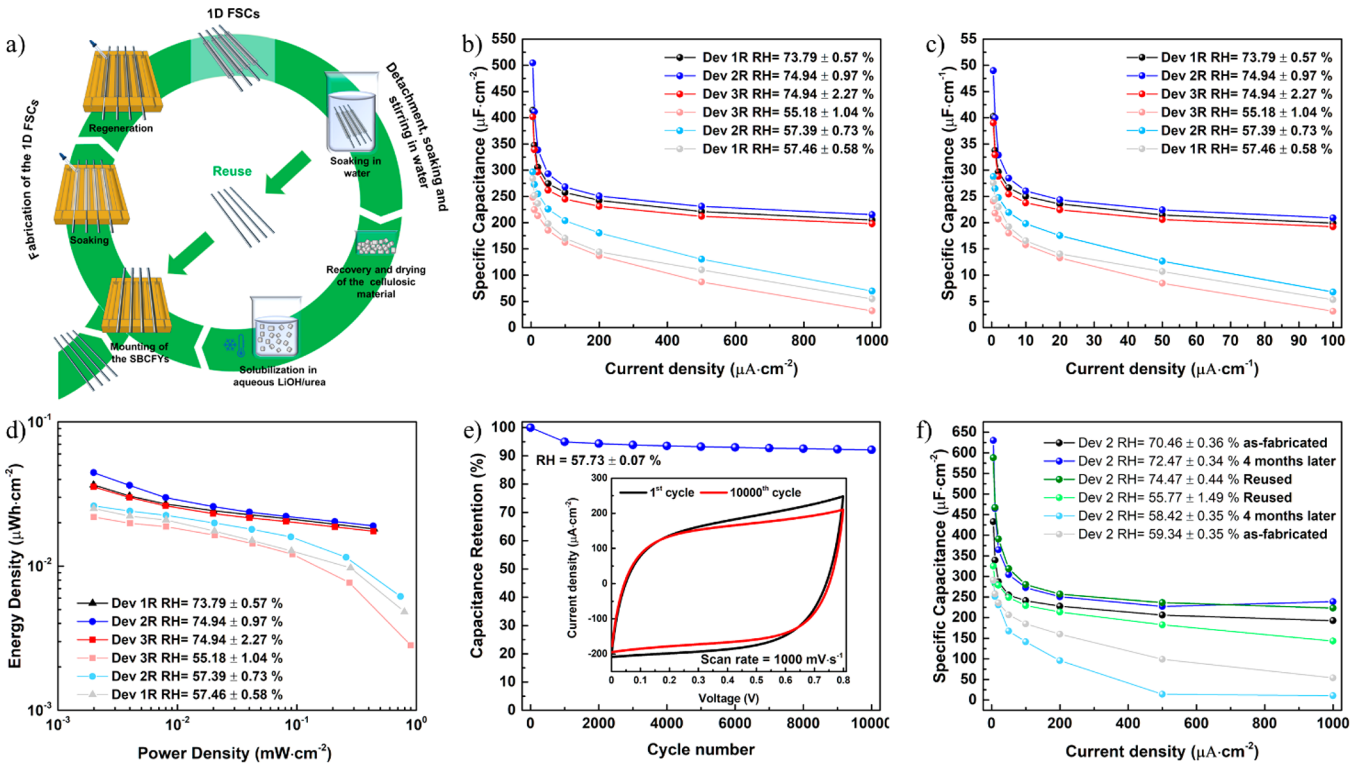

Figure 6. (a) Schematic summary of the followed circular approach, for the produced 1D FSCs: (b) the areal and (c) the length-specific capacitances measured at different current densities, ranging from 5 to 1000 $\mu A \cdot cm^{-2}$ and 0.5 to 100 $\mu A \cdot cm^{-1}$, for three RRCIH 1D FSCs at both RH levels, within an operating voltage window of 0.8 V, respectively. (d) The respective Ragone plot, (e) the cycling performance, at a scan rate of 1000 $mV \cdot s^{-1}$, for 10 000 CV cycles, in a voltage window of 0.8 V and an RH of 57.73 ± 0.07%, (f) a comparison of the determined specific capacitances, for the same 1D FSCs as fabricated, 4 months later and reused, ranging from 5 to 1000 $\mu A \cdot cm^{-2}$, within an operating voltage window of 0.8 V.

1.73×10^{-2} $\mu Wh \cdot cm^{-2}$ at a power density of 5.33×10^{-1} $mW \cdot cm^{-2}$ and 2.47×10^{-3} $\mu Wh \cdot cm^{-1}$ at 7.61×10^{-2} $mW \cdot cm^{-1}$. Figure S8 shows the energy and power density of the RCIHs for an operating voltage window of 0.6 V.

Another important consideration about the produced 1D FSCs is their long-term stability. The devices could sustain up to 92% of their initial capacitance after performing 10 000 CV cycles at 1000 $mV \cdot s^{-1}$, as represented in Figure 5c, and up to 84.5% for an RH = 77.63%, as shown in Figure S9. Additionally, the integration of the produced 1D FSCs was demonstrated by connecting three devices in series and parallel, respectively (Figure 5d,e) Lastly, Figure 5f presents the variation of the current density for the 1D FSCs, acquired at 100 $mV \cdot s^{-1}$, in flat and bent positions, as shown in Figure S10. Mechanical bending executing 50, 100, 200, 600, and 1000 cycles was performed by hand over a mold, with a bending radius of 45 mm, as shown in Figure S11. The electrochemical characterization performed after each cycle indicates a gradual decrease in the CV area, meaning a decrease in capacitance. Also, as evidenced in the bode plot, the impedance increases at high frequencies. This could be related by the appearance of cracks after 50 bending cycles, as shown in Figure S11e. Moreover, after 1000 bending cycles, it is still possible to see parts of the device (Figure S11f) that have not yet been compromised and others where the number of cracks has increased (Figure S11g,h). Nevertheless, after 1000 cycles, the devices' capacitance seems to stabilize. For further improvement of the mechanical performance, an encapsulation layer might be considered so the device can undergo greater deformations without the formation of cracks and less sensitive to variations in the RH.

To demonstrate the applicability of the fabricated devices, six 1D FSCs were weaved in a woven textile and connected in series to light up three red LEDs and one thermometer, as displayed in Figure S12.

Finally, by considering a circular approach, the end-of-life of the produced 1D FSCs was handled in two distinct directions, as summarized in Figure 6a. First, the fabricated 1D FSCs were washed with deionized water to remove the remaining salts from the RCIHs, and it was detached from the SBCFYs. Both were allowed to dry at 40 °C and stored at room temperature. Afterward, the dried cellulose was reused to prepare a solution of 5 wt % recovered material in a new precooled aqueous LiOH/urea solvent system, using the previous solubilization strategy for MCC. New 1D FSCs were fabricated using recycled regenerated cellulose-based ionic hydrogels (RRCIHs).

Figure 6b,c depicts the C_s per area and length over the applied current densities for three 1D FSCs with RRCIHs, considering both RH levels and an operating voltage window of 0.8 V. In terms of the electrochemical performance, the new 1D FSCs have C_s values in the same order of magnitude as those using the pristine electrolyte RCIHs, as depicted in Table S1. Additionally, even at high current densities (1 $mA \cdot cm^{-2}$), the devices display a C_s greater than 197 $\mu F \cdot cm^{-2}$, and the maximum achieved power density was 4.36×10^{-1} $mW \cdot cm^{-2}$ with an energy density of 1.90×10^{-2} $\mu Wh \cdot cm^{-2}$.

The long-term stability was also verified in the RRCIH 1D FSCs, showing that they can sustain 92% of their initial

https://doi.org/10.1021/acsaem.2c01222
ACS Appl. Energy Mater. 2022, 5, 11987−11996

capacitance after performing 10 000 CV cycles at 1000 $mV{\cdot}s^{-1}$, as represented in Figure 6e, and sustain 74.8% for an RH = 78.50%, as shown in Figure S13. This more pronounced loss at higher RH, for the 1D FSCs with RRCIHs, can be related to the recycling procedure. Nevertheless, after 1000 CV cycles the capacitance seems to stabilize, indicating that no further changes are induced in the device. Lastly, Figure 6f depicts the C_s for the same 1D FSCs after being fabricated, 4 months later, and obtained from reused materials. For the last, the recovered SBCFYs were reused to fabricate new planar 1D FSCs using the RRCIHs, as the electrolyte, following the same fabrication procedure for the pristine devices (Figure 6a). After 4 months the device shows stable C_s for the higher RH level. The reused and recycled 1D FSCs depicts a slight increased C_s which can be related to the presence of reminiscent ionic species adsorbed on the SBCFY and cotton yarns, as shown in Figure S14.

In Table S2 we compare our fabricated 1D FSCs with other related works based on CFs with the same configuration and electrodes. Even though both power and energy densities are inferior to the reported ones, it is important to notice that even at 10 000 $mV{\cdot}s^{-1}$ our 1D FSCs can sustain the typical EDLC quasi-rectangular behavior. Despite presenting higher charge storage capabilities, the compared systems shown in Table S2 lose their electrochemical performance at much lower scan rates. Furthermore, we present a sustainable approach considering the use of low-cost, well-established, and commercially available carbon fibers that can be reused to produce new devices. Additionally, a regenerated cellulose-based ionic hydrogel (RCIH) is addressed as an alternative electrolyte, able to be regenerated in a tubular form around the SBCFYs which are recovered from the electrodes and reused.

4. CONCLUSIONS

We report a facile fabrication methodology of flexible and sustainable 1D FSC energy storage devices using commercially available SBCFYs as current collectors with *in situ* regenerated cellulose-based ionic hydrogels (RCIHs) as electrolytes. The hydrophilic nature of the cellulose makes the electrolyte susceptible to humidity changes which strongly influences the electrochemical performance of the 1D FSCs. An increase in the specific capacitance and energy density and a decrease in the ESR are observed for higher relative humidity. The long-term stability is preserved with 92% of its initial capacitance after performing 10 000 CV cycles at 1000 $mV{\cdot}s^{-1}$. Additionally, it was demonstrated that the 1D FSCs maintain their functionality after 4 months, and it was possible to weave them into a textile and light up three red LEDs.

By implementing a successful circular approach, it is possible to reuse both the SBCFYs and the cellulose-based electrolyte to fabricate new 1D FSCs without significant performance loss. Soon, we foresee such sustainable approaches being more present in the recovery of high-value compounds to fully develop sustainable energy-storage systems for wearable IoT electronics.

■ ASSOCIATED CONTENT

Supporting Information

The Supporting Information is available free of charge at https://pubs.acs.org/doi/10.1021/acsaem.2c01222.

Main features of the SBCFY; evolution of the electrochemical stable potential window; comparison between the produced 1D FSCs using regenerated cellulose-based ionic hydrogels (RCIHs) and PVA/H_3PO_4, as electrolytes, concerning Cs and ESR for both RH levels; CV and GCD curves of the produced 1D FSCs with PVA/H_3PO_4, as well as the areal specific capacitance for both RH levels; images of six 1D FSCs connected in series, weaved in a cotton textile, lighting up three red LEDs and one thermometer; electrochemical calculations; and comparison between the produced 1D FSCs using the regenerated cellulose-based ionic hydrogels (RCIHs) and PVA/H_3PO_4 as electrolytes with the literature (PDF)

■ AUTHOR INFORMATION

Corresponding Author

Luís Pereira − *CENIMAT|i3N, Department of Materials Science, School of Science and Technology, NOVA University Lisbon and CEMOP/UNINOVA, Caparica 2829-516, Portugal; AlmaScience, Caparica 2829-516, Portugal;* orcid.org/0000-0001-8281-8663; Email: lmnp@fct.unl.pt

Authors

José Tiago Carvalho − *CENIMAT|i3N, Department of Materials Science, School of Science and Technology, NOVA University Lisbon and CEMOP/UNINOVA, Caparica 2829-516, Portugal;* orcid.org/0000-0002-6654-8859

Inês Cunha − *CENIMAT|i3N, Department of Materials Science, School of Science and Technology, NOVA University Lisbon and CEMOP/UNINOVA, Caparica 2829-516, Portugal*

João Coelho − *CENIMAT|i3N, Department of Materials Science, School of Science and Technology, NOVA University Lisbon and CEMOP/UNINOVA, Caparica 2829-516, Portugal;* orcid.org/0000-0003-4217-3842

Elvira Fortunato − *CENIMAT|i3N, Department of Materials Science, School of Science and Technology, NOVA University Lisbon and CEMOP/UNINOVA, Caparica 2829-516, Portugal;* orcid.org/0000-0002-4202-7047

Rodrigo Martins − *CENIMAT|i3N, Department of Materials Science, School of Science and Technology, NOVA University Lisbon and CEMOP/UNINOVA, Caparica 2829-516, Portugal*

Complete contact information is available at: https://pubs.acs.org/10.1021/acsaem.2c01222

Author Contributions

José Tiago Carvalho: Methodology, Investigation, Data Curation, Visualization, and Writing—original draft. Ines Cunha: Methodology, Investigation, Curation, Writing—original draft. João Coelho: Data Curation, Writing—reviewing and editing. Elvira Fortunato: Writing—reviewing and editing, Project administration, Funding acquisition. Rodrigo Martins: Writing—reviewing and editing, Supervision, Project administration, Funding acquisition. Luís Pereira: Conceptualization, Writing—reviewing and editing, Supervision, Project administration, Funding acquisition.

Notes

The authors declare no competing financial interest.

https://doi.org/10.1021/acsaem.2c01222
ACS Appl. Energy Mater. 2022, 5, 11987−11996

■ ACKNOWLEDGMENTS

This work was financed by national funds from FCT - Fundação para a Ciência e a Tecnologia, I.P., in the scope of the projects LA/P/0037/2020, UIDP/50025/2020, and UIDB/50025/2020 of the Associate Laboratory Institute of Nanostructures, Nanomodeling and Nanofabrication−i3N, and by projects PTDC/NAN-MAT/32558/2017 and PTDC/CTM-PAM/4241/2020. J.T.C. acknowledges the support from the Portuguese Foundation for Science and Technology under the scholarship SFRH/BD/139225/2018 and IDS-FunMat-INNO project FPA2016/EIT/EIT RawMaterials Grant Agreement 17184. I.C. acknowledges the Portuguese Foundation for Science and Technology for the PhD scholarship SFRH/BD/126409/2016. This work has received funding from the European Union's Horizon 2020 Research and Innovation Programme under the Grant Agreements Nos.: 640598 (ERC-2014-STG NEW-FUN), 952169 (SYNERGY, H2020-WIDESPREAD-2020-5, CSA), and 101008701 (EMERGE, H2020-INFRAIA-2020-1). The authors would also like to thank Daniela Gomes, Sofia Ferreira, and Sara Silvestre from CENIMAT|i3N for their contribution to SEM, XRD measurements, and 3D printing, respectively. We would like to thank Julia Cramer and Kay Ullrich from TITV for providing the necessary tools to twist the cotton yarn.

■ REFERENCES

(1) Stoppa, M.; Chiolerio, A. Wearable Electronics and Smart Textiles: A Critical Review. *Sensors* **2014**, *14*, 11957−11992.
(2) Shi, J.; Liu, S.; Zhang, L.; Yang, B.; Shu, L.; Yang, Y.; Ren, M.; Wang, Y.; Chen, J.; Chen, W.; Chai, Y.; Tao, X. Smart Textile-Integrated Microelectronic Systems for Wearable Applications. *Adv. Mater.* **2020**, *32*, 1901958.
(3) Commission, E. Communication COM(2020) 474 final: Critical Raw Materials Resilience: Charting a Path towards greater Security and Sustainability. https://eur-lex.europa.eu/legal-content/EN/TXT/?uri=CELEX%3A52020DC0474 (accessed 2020).
(4) Parajuly, K.; Fitzpatrick, C.; Muldoon, O.; Kuehr, R. Behavioral change for the circular economy: A review with focus on electronic waste management in the EU. *Resour. Conserv. Recycl. X* **2020**, *6*, 100035.
(5) Nandy, S.; Fortunato, E.; Martins, R. Green economy and waste management: An inevitable plan for materials science. *Prog. Nat. Sci. Mater. Int.* **2022**, *32*, 1−9.
(6) Bao, L.; Li, X. Towards Textile Energy Storage from Cotton T-Shirts. *Adv. Mater.* **2012**, *24*, 3246−3252.
(7) Gao, Z.; Song, N.; Zhang, Y.; Li, X. Cotton textile enabled, all-solid-state flexible supercapacitors. *RSC Adv.* **2015**, *5*, 15438−15447.
(8) Huang, Y.; Chen, J. Y. All-carbon cord-yarn supercapacitor. *J. Ind. Text.* **2018**, *48*, 875−883.
(9) Lima, N.; Baptista, A. C.; Faustino, B. M. M.; Taborda, S.; Marques, A.; Ferreira, I. Carbon threads sweat-based supercapacitors for electronic textiles. *Sci. Rep.* **2020**, *10*, 7703.
(10) Zhai, S.; Jiang, W.; Wei, L.; Karahan, H. E.; Yuan, Y.; Ng, A. K.; Chen, Y. All-carbon solid-state yarn supercapacitors from activated carbon and carbon fibers for smart textiles. *Mater. Horizons* **2015**, *2*, 598−605.
(11) Shen, C.; Xie, Y.; Zhu, B.; Sanghadasa, M.; Tang, Y.; Lin, L. Wearable woven supercapacitor fabrics with high energy density and load-bearing capability. *Sci. Rep.* **2017**, *7*, 14324.
(12) Le, V. T.; Kim, H.; Ghosh, A.; Kim, J.; Chang, J.; Vu, Q. A.; Pham, D. T.; Lee, J.-H.; Kim, S.-W.; Lee, Y. H. Coaxial Fiber Supercapacitor Using All-Carbon Material Electrodes. *ACS Nano* **2013**, *7*, 5940−5947.
(13) Zhang, C.; Chen, Z.; Rao, W.; Fan, L.; Xia, Z.; Xu, W.; Xu, J. A high-performance all-solid-state yarn supercapacitor based on polypyrrole-coated stainless steel/cotton blended yarns. *Cellulose* **2019**, *26*, 1169−1181.
(14) Lamberti, A.; Gigot, A.; Bianco, S.; Fontana, M.; Castellino, M.; Tresso, E.; Pirri, C. F. Self-assembly of graphene aerogel on copper wire for wearable fiber-shaped supercapacitors. *Carbon N. Y.* **2016**, *105*, 649−654.
(15) Jost, K.; Dion, G.; Gogotsi, Y. Textile energy storage in perspective. *J. Mater. Chem. A* **2014**, *2*, 10776.
(16) Ismar, E.; Kurşun Bahadir, S.; Kalaoglu, F.; Koncar, V. Futuristic Clothes: Electronic Textiles and Wearable Technologies. *Glob. Challenges* **2020**, *4*, 1900092.
(17) Ghouri, A. S.; Aslam, R.; Siddiqui, M. S.; Sami, S. K. Recent Progress in Textile-Based Flexible Supercapacitor. *Front. Mater.* **2020**, *7*, 1−7.
(18) Zhou, Y.; Wang, C.; Lu, W.; Dai, L. Recent Advances in Fiber-Shaped Supercapacitors and Lithium-Ion Batteries. *Adv. Mater.* **2020**, *32*, 1902779.
(19) Zhai, S.; Karahan, H. E.; Wang, C.; Pei, Z.; Wei, L.; Chen, Y. 1D Supercapacitors for Emerging Electronics: Current Status and Future Directions. *Adv. Mater.* **2020**, *32*, 1902387.
(20) Gulzar, U.; Goriparti, S.; Miele, E.; Li, T.; Maidecchi, G.; Toma, A.; De Angelis, F.; Capiglia, C.; Zaccaria, R. P. Next-generation textiles: from embedded supercapacitors to lithium ion batteries. *J. Mater. Chem. A* **2016**, *4*, 16771−16800.
(21) Chen, S.; Qiu, L.; Cheng, H.-M. Carbon-Based Fibers for Advanced Electrochemical Energy Storage Devices. *Chem. Rev.* **2020**, *120*, 2811−2878.
(22) Gao, L.; Li, X.; Li, X.; Cheng, J.; Wang, B.; Wang, Z.; Li, C. A coaxial yarn electrode based on hierarchical MoS 2 nanosheets/carbon fiber tows for flexible solid-state supercapacitors. *RSC Adv.* **2016**, *6*, 57190−57198.
(23) Nandy, S.; Goswami, S.; Marques, A.; Gaspar, D.; Grey, P.; Cunha, I.; Nunes, D.; Pimentel, A.; Igreja, R.; Barquinha, P.; Pereira, L.; Fortunato, E.; Martins, R. Cellulose: A Contribution for the Zero e-Waste Challenge. *Adv. Mater. Technol.* **2021**, *6*, 2000994.
(24) Pérez-Madrigal, M. M.; Edo, M. G.; Alemán, C. Powering the future: application of cellulose-based materials for supercapacitors. *Green Chem.* **2016**, *18*, 5930−5956.
(25) Shen, X.; Shamshina, J. L.; Berton, P.; Gurau, G.; Rogers, R. D. Hydrogels based on cellulose and chitin: fabrication, properties, and applications. *Green Chem.* **2016**, *18*, 53−75.
(26) Fu, L.-H.; Qi, C.; Ma, M.-G.; Wan, P. Multifunctional cellulose-based hydrogels for biomedical applications. *J. Mater. Chem. B* **2019**, *7*, 1541−1562.
(27) El Seoud, O. A.; Kostag, M.; Jedvert, K.; Malek, N. I. Cellulose Regeneration and Chemical Recycling: Closing the "Cellulose Gap" Using Environmentally Benign Solvents. *Macromol. Mater. Eng.* **2020**, *305*, 1900832.
(28) Yang, Q.; Fukuzumi, H.; Saito, T.; Isogai, A.; Zhang, L. Transparent Cellulose Films with High Gas Barrier Properties Fabricated from Aqueous Alkali/Urea Solutions. *Biomacromolecules* **2011**, *12*, 2766−2771.
(29) He, M.; Zhao, Y.; Duan, J.; Wang, Z.; Chen, Y.; Zhang, L. Fast Contact of Solid−Liquid Interface Created High Strength Multi-Layered Cellulose Hydrogels with Controllable Size. *ACS Appl. Mater. Interfaces* **2014**, *6*, 1872−1878.
(30) Cunha, I.; Barras, R.; Grey, P.; Gaspar, D.; Fortunato, E.; Martins, R.; Pereira, L. Reusable Cellulose-Based Hydrogel Sticker Film Applied as Gate Dielectric in Paper Electrolyte-Gated Transistors. *Adv. Funct. Mater.* **2017**, *27*, 1606755.
(31) Cunha, I.; Martins, J.; Gaspar, D.; Bahubalindruni, P. G.; Fortunato, E.; Martins, R.; Pereira, L. Healable Cellulose Iontronic Hydrogel Stickers for Sustainable Electronics on Paper. *Adv. Electron. Mater.* **2021**, *7*, 2001166.
(32) Cunha, I.; Martins, J.; Bahubalindruni, P. G.; Carvalho, J. T.; Rodrigues, J.; Rubin, S.; Fortunato, E.; Martins, R.; Pereira, L. Handwritten and Sustainable Electronic Logic Circuits with Fully Printed Paper Transistors. *Adv. Mater. Technol.* **2021**, *6*, 2100633.

https://doi.org/10.1021/acsaem.2c01222
ACS Appl. Energy Mater. 2022, 5, 11987−11996

(33) Chen, D.; Jiang, K.; Huang, T.; Shen, G. Recent Advances in Fiber Supercapacitors: Materials, Device Configurations, and Applications. *Adv. Mater.* **2020**, *32*, 1901806.
(34) Wang, L.; Fu, X.; He, J.; Shi, X.; Chen, T.; Chen, P.; Wang, B.; Peng, H. Application Challenges in Fiber and Textile Electronics. *Adv. Mater.* **2020**, *32*, 1901971.
(35) Wang, C.; Xia, K.; Wang, H.; Liang, X.; Yin, Z.; Zhang, Y. Advanced Carbon for Flexible and Wearable Electronics. *Adv. Mater.* **2019**, *31*, 1801072.
(36) Cai, J.; Zhang, L.; Liu, S.; Liu, Y.; Xu, X.; Chen, X.; Chu, B.; Guo, X.; Xu, J.; Cheng, H.; Han, C. C.; Kuga, S. Dynamic Self-Assembly Induced Rapid Dissolution of Cellulose at Low Temperatures. *Macromolecules* **2008**, *41*, 9345−9351.
(37) Cai, J.; Zhang, L.; Chang, C.; Cheng, G.; Chen, X.; Chu, B. Hydrogen-Bond-Induced Inclusion Complex in Aqueous Cellulose/LiOH/Urea Solution at Low Temperature. *ChemPhysChem* **2007**, *8*, 1572−1579.
(38) Luo, X.; Zhang, L. New solvents and functional materials prepared from cellulose solutions in alkali/urea aqueous system. *Food Res. Int.* **2013**, *52*, 387−400.
(39) Cai, J.; Zhang, L. Rapid Dissolution of Cellulose in LiOH/Urea and NaOH/Urea Aqueous Solutions. *Macromol. Biosci.* **2005**, *5*, 539−548.
(40) Medronho, B.; Lindman, B. Brief overview on cellulose dissolution/regeneration interactions and mechanisms. *Adv. Colloid Interface Sci.* **2015**, *222*, 502−508.
(41) Oh, S. Y.; Yoo, D.; Il; Shin, Y.; Kim, H. C.; Kim, H. Y.; Chung, Y. S.; Park, W. H.; Youk, J. H. Crystalline structure analysis of cellulose treated with sodium hydroxide and carbon dioxide by means of X-ray diffraction and FTIR spectroscopy. *Carbohydr. Res.* **2005**, *340*, 2376−2391.
(42) Dong, Y.; Hou, L.; Wu, P. Exploring the diffusion behavior of urea aqueous solution in the viscose film by ATR-FTIR spectroscopy. *Cellulose* **2020**, *27*, 2403−2415.
(43) Mafy, N. N.; Afrin, T.; Rahman, M. M.; Mollah, M. Y. A.; Susan, M. A. B. H. Effect of temperature perturbation on hydrogen bonding in aqueous solutions of different urea concentrations. *RSC Adv.* **2015**, *5*, 59263−59272.
(44) Mathis, T. S.; Kurra, N.; Wang, X.; Pinto, D.; Simon, P.; Gogotsi, Y. Energy Storage Data Reporting in Perspective—Guidelines for Interpreting the Performance of Electrochemical Energy Storage Systems. *Adv. Energy Mater.* **2019**, *9*, 1902007.
(45) Wang, Z.; Li, H.; Tang, Z.; Liu, Z.; Ruan, Z.; Ma, L.; Yang, Q.; Wang, D.; Zhi, C. Hydrogel Electrolytes for Flexible Aqueous Energy Storage Devices. *Adv. Funct. Mater.* **2018**, *28*, 1804560.
(46) Miao, L.; Song, Z.; Zhu, D.; Li, L.; Gan, L.; Liu, M. Recent advances in carbon-based supercapacitors. *Mater. Adv.* **2020**, *1*, 945−966.
(47) Zhang, S.; Pan, N. Supercapacitors Performance Evaluation. *Adv. Energy Mater.* **2015**, *5*, 1401401.

https://doi.org/10.1021/acsaem.2c01222
ACS Appl. Energy Mater. 2022, 5, 11987−11996